J|A|C|S ARTICLES

Published on Web 07/15/2010

The Histidine Effect. Electron Transfer and Capture Cause Different Dissociations and Rearrangements of Histidine Peptide Cation-Radicals

František Tureček,*,§ Thomas W. Chung,§ Christopher L. Moss,§ Jean A. Wyer,# Anneli Ehlerding,# Anne I. S. Holm,# Henning Zettergren,# Steen Brøndsted Nielsen,# Preben Hvelplund,# Julia Chamot-Rooke,† Benjamin Bythell,‡ and Béla Paizs‡

Department of Chemistry, Bagley Hall, Box 351700, University of Washington, Seattle, Washington 98195-1700, Department of Physics and Astronomy, University of Aarhus, DK-8000 Aarhus, Denmark, Laboratory of Reaction Mechanisms, Ecole Polytechnique, 91128 Palaiseau, France, and German Cancer Research Center, D-69120 Heidelberg, Germany

Received September 14, 2009; E-mail: turecek@chem.washington.edu

Abstract: Electron-transfer and -capture dissociations of doubly protonated peptides gave dramatically different product ions for a series of histidine-containing pentapeptides of both non-tryptic (AAHAL, AHAAL, AHADL, AHDAL) and tryptic (AAAHK, AAHAK, AHAAK, HAAAK, AAAHR, AAHAR, AHAAR, HAAAR) type. Electron transfer from gaseous Cs atoms and fluoranthene anions triggered backbone dissociations of all four N−C_α bonds in the peptide ions in addition to loss of H and NH_3. Substantial fractions of charge-reduced cation-radicals did not dissociate on an experimental time scale ranging from 10^{-6} to 10^{-1} s. Multistage tandem mass spectrometric (MS^n) experiments indicated that the non-dissociating cation-radicals had undergone rearrangements. These were explained as being due to proton migrations from N-terminal ammonium and COOH groups to the C-2′ position of the reduced His ring, resulting in substantial radical stabilization. Ab initio calculations revealed that the charge-reduced cation-radicals can exist as low-energy zwitterionic amide π^* states which were local energy minima. These states underwent facile exothermic proton migrations to form aminoketyl radical intermediates, whereas direct N−C_α bond cleavage in zwitterions was disfavored. RRKM analysis indicated that backbone N−C_α bond cleavages did not occur competitively from a single charge-reduced precursor. Rather, these bond cleavages proceeded from distinct intermediates which originated from different electronic states accessed by electron transfer. In stark contrast to electron transfer, capture of a free electron by the peptide ions mainly induced radical dissociations of the charge-carrying side chains and loss of a hydrogen atom followed by standard backbone dissociations of even-electron ions. The differences in dissociation are explained by different electronic states being accessed upon electron transfer and capture.

Introduction

Protein sequencing by mass spectrometry is critically dependent on the way amino acid residues affect fragmentations of gas-phase ions.[1] For example, charge-induced dissociations of even-electron peptide ions are substantially affected by amino acid residues exhibiting high basicity (Arg),[2] having a tendency to stabilize specific ion fragments (Pro),[3] or promoting amide bond dissociations by neighboring group participation (Asp).[4] With the advent of electron-based methods of peptide and protein analysis, efforts have been made to reveal the effects of amino acid residues on dissociations of peptide cation-radicals produced by electron capture or transfer. Such peptide cation-radicals tend to undergo dissociations involving cleavage of bonds between the amide nitrogen atom and the C_α atom of the adjacent residue, an N−C_α cleavage for short.[5] Several model peptides have been investigated using electron-capture dissociation (ECD)[6] and electron-transfer dissociation (ETD),[7] in which

§ University of Washington.
# University of Aarhus.
† Ecole Polytechnique.
‡ German Cancer Research Center.

(1) Paizs, B.; Suhai, S. *Mass Spectrom. Rev.* **2005**, *24*, 508–548.
(2) (a) Wysocki, V. H.; Tsapralis, G.; Smith, L. L.; Breci, L. A. *J. Mass Spectrom.* **2000**, *35*, 1399–1406. (b) Tsaprailis, G.; Nair, H.; Somogyi, A.; Wysocki, V. H.; Zhong, W.; Futrell, J. H.; Summerfield, S. G.; Gaskell, S. J. *J. Am. Chem. Soc.* **1999**, *121*, 5142–5154. (c) Bythell, B. J.; Suhai, S.; Somogyi, A.; Paizs, B. *J. Am. Chem. Soc.* **2009**, *131*, 14057–14065.
(3) (a) Vaisar, T.; Urban, J. *J. Mass Spectrom.* **1996**, *31*, 1185–1187. (b) Grewal, R. N.; El Aribi, H.; Harrison, A. G.; Siu, K. W. M.; Hopkinson, A. C. *J. Phys. Chem. B* **2004**, *108*, 4899–4908.
(4) (a) Yu, W.; Vath, J. E.; Huberty, M. C.; Martin, S. A. *Anal. Chem.* **1993**, *65*, 3015–3023. (b) Qin, J.; Chait, B. T. *J. Am. Chem. Soc.* **1995**, *117*, 5411–5412. (c) Lee, S.-W.; Kim, H. S.; Beauchamp, J. L. *J. Am. Chem. Soc.* **1998**, *120*, 3188–3195.
(5) Zubarev, R. A.; Horn, D. M.; Fridriksson, E. K.; Kelleher, N. L.; Kruger, N. A.; Lewis, M. A.; Carpenter, B. K.; McLafferty, F. W. *Anal. Chem.* **2000**, *72*, 563–573.
(6) Zubarev, R. A.; Kelleher, N. L.; McLafferty, F. W. *J. Am. Chem. Soc.* **1998**, *120*, 3265–3266.
(7) Syka, J. E. P.; Coon, J. J.; Schroeder, M. J.; Shabanowitz, J.; Hunt, D. H. *Proc. Natl. Acad. Sci. U.S.A.* **2004**, *101*, 9528–9533.

 10.1021/ja907808h

specific amino acid residues have been varied while maintaining the rest of the peptide sequence the same. For example, Fung and Chan have reported an ECD study of several nonapeptides of the RGGGXGGGR type to explore radical side-chain losses from the X residue.[8] Cooper investigated the effect on backbone dissociations of Arg and Lys residues in ECD.[9] Effects on electron-induced backbone dissociations of peptide secondary structure[10] and the presence of basic[11] and hydrophobic amino acid residues[12] have been investigated. In addition, a statistical approach has been applied to classify electron-induced dissociations of a large set of tryptic peptides and extract regularities in the backbone dissociations[13] and eliminations of small neutral molecules.[14]

Recently, Xia et al. investigated the effect of basic amino acid residues (Arg, Lys, His) on ETD of small peptides.[15] They observed unusual behavior of peptide trications containing His residues which were efficiently reduced by electron transfer; however, a substantial fraction of the cation-radicals formed then failed to dissociate. No such effect was observed for Lys- and Arg-containing peptides,[15] pointing to some unusual properties of protonated His residues upon electron transfer. We have studied this effect for His-containing di- and tripeptide monocations which were reduced by collisional electron transfer from cesium atoms and the neutral radical intermediates were analyzed by collisional re-ionization to anions.[16] A mechanism was proposed to explain the stability of His-containing radicals which involved a carboxyl-catalyzed prototropic rearrangement in the imidazolium ring, which resulted in a substantial stabilization of the intermediates and suppression of their backbone dissociations.[17] The basic question which has remained unresolved was whether similar rearrangements play a role in the stabilization of His-containing cation-radicals of relevance to protein sequencing by ECD and ETD. To address this issue, we carried out a joint experimental and computational study of several histidine-containing pentapeptides. Here we report results for *non-tryptic* pentapeptides AAHAL, AHAAL, AHDAL, and AHADL, as well as for two series of peptides of a *tryptic* type,[18] AAAHX, AAHAX, AHAAX, and HAAAX, where X is arginine (R) or lysine (K).[19] All these peptides form abundant doubly charged ions upon electrospray ionization. However, the protonation sites differ in that the non-tryptic peptides are protonated in the His ring and at the N-terminal amino group, whereas the tryptic peptides are protonated in the His ring and at the basic C-terminal residue (K or R).[20] The carboxyl as well as ammonium groups can serve as proton donors in the catalyzed isomerization. The doubly charged ions are subjected to charge reduction under three different experimental conditions: (1) femtosecond collisional electron transfer from gaseous cesium atoms for ions from AAHAL, AHDAL, and AHADL; (2) ion−ion reactions with fluoranthene anion-radicals as electron donors; and (3) capture of free low-energy electrons for all peptide ions. Analysis of product ions by multistage tandem mass spectrometry (MS^n) is combined with ab initio quantum chemical exploration of the potential energy surface (PES) and Rice−Ramsperger−Kassel−Marcus (RRKM) calculations of unimolecular rate constants for selected peptide ions to rationalize the experimentally observed phenomena.

Experimental Section

Materials and Methods. Peptides AHDAL, AHADL, and AAHAL (>95% pure) were custom synthesized by GenScript (Piscataway, NJ), and the other peptides (98% pure) were purchased from NEO-Group (Cambridge, MA). In each case the peptide sequence was confirmed by tandem mass spectra. Doubly charged ions were produced by electrospray ionization of solutions in 50/50 methanol−water containing 1% acetic acid. Electron-capture induced dissociation (ECID) mass spectra were measured on a large-scale sector instrument described previously.[21] Precursor ions were accelerated to 100 keV, selected by mass, and allowed to collide with cesium atoms under mostly single-collision conditions. Charge-reduced products were separated by an electrostatic sector analyzer and detected by ion counting. Electron-transfer dissociation (ETD) mass spectra were measured on a Thermo Scientific (San Jose, CA) LTQ-ETD linear ion trap instrument equipped with a chemical ionization source for the production of fluoranthene anion-radicals as ETD reagent. Precursor dications were selected by mass, with a 2 mass unit (mu) window, and allowed to react with fluoranthene anions for 100 or 200 ms. Multistage tandem mass spectrometry was performed by selecting a charge-reduced ion from the ETD spectrum, followed by its collisional activation with the bath gas at 50−60% of radio frequency power. Electron-capture dissociation (ECD) mass spectra were measured on a Thermo Scientific (San Jose, CA) LTQ Fourier transform (FT) ion cyclotron resonance (ICR) mass spectrometer. Precursor ions were selected in the linear ion trap with a 2 mu window, transferred to the ICR cell, and irradiated by electrons from an external source. The electron energy cannot be measured accurately on the Thermo instrument, and so only nominal potential values were varied between 3 and 5 V. The irradiation time was varied between 100 and 500 ms. Infrared multiphoton dissociation (IRMPD) mass spectra of singly protonated peptides were also measured on the LTQ-FT-MS instrument using a CO_2 laser at 40−50% beam attenuation. The ECD spectra were re-measured on a Bruker Daltonik (Bremen, Germany) 7-T APEX III FT-ICR mass spectrometer equipped with a hexapole ion trap as reported previously.[22] Ions trapped in the ICR cell were irradiated with electrons from an external cathode. The electron energy was

(8) Fung, Y. M. E.; Chan, T.-W. D. *J. Am. Soc. Mass Spectrom.* **2005**, *16*, 1523–1535.
(9) Cooper, H. J. *J. Am. Soc. Mass Spectrom.* **2005**, *16*, 1932–1940.
(10) Patriksson, A.; Adams, C.; Kjeldsen, F.; Raber, J.; van der Spoel, D.; Zubarev, R. A. *Int. J. Mass Spectrom.* **2006**, *248*, 124–135.
(11) Tsybin, Y. O.; Haselmann, K. F.; Emmett, M. R.; Hendrickson, C. L.; Marshall, A. G. *J. Am. Soc. Mass Spectrom.* **2006**, *17*, 1704–1711.
(12) Ben Hamidame, H.; He, H.; Tsybin, O. Yu.; Emmett, M. R.; Hendrickson, C. L.; Marshall, A. G.; Tsybin, Y. O. *J. Am. Soc. Mass Spectrom.* **2009**, *20*, 1182–1192.
(13) Savitskii, M. M.; Kjeldsen, F.; Nielsen, M. L.; Zubarev, R. A. *Angew. Chem., Int. Ed.* **2006**, *45*, 5301–5303.
(14) Faelth, M.; Savitski, M. M.; Nielsen, M. L.; Kjeldsen, F.; Andren, P. E.; Zubarev, R. A. *Anal. Chem.* **2008**, *80*, 8089–8094.
(15) Xia, Y.; Gunawardena, H. P.; Erickson, D. E.; McLuckey, S. A. *J. Am. Chem. Soc.* **2007**, *129*, 12232–12243.
(16) Tureček, F.; Jones, J. W.; Towle, T.; Panja, S.; Nielsen, S. B.; Hvelplund, P.; Paizs, B. *J. Am. Chem. Soc.* **2008**, *130*, 14584–14596.
(17) Tureček, F.; Yao, C.; Fung, Y. M. E.; Hayakawa, S.; Hashimoto, M.; Matsubara, H. *J. Phys. Chem. B* **2009**, *113*, 7347–7366.
(18) Whereas the sequences of the tryptic-type peptides were selected to vary the position of the His residue, a protein database search (http://www.uniprot.org) found 1040 proteins that would produce these peptides upon trypsinolysis.
(19) Several tryptic pentapeptides containing phosphoserine (pSAAAX, ApSAAX, AApSAX, and AAApSX, where X = R or K) showed ECD and ETD spectra that were quite analogous to those reported here for the histidine-containing pentapeptides. These results are beyond the scope of the present work and will be reported separately.
(20) A reviewer raised a question of His versus N-terminal protonation in AAAHK and AAAHR. Our exhaustive structure analysis of the conformational space for N-terminal and His-protonated tautomers of $(AAAHR + 2H)^{2+}$ ions, followed by full B3LYP/6-31+G(d,p) optimization and B3LYP and MP2 single-point energy calculations, found His-protonated structures to have lower enthalpies and free energies than the N-terminal protonated tautomers.
(21) Boltalina, O. V.; Hvelplund, P.; Jørgensen, T. J. D.; Larsen, M. C.; Larsson, M. O.; Sharoitchenko, D. A.; Sørensen, M. *Phys. Rev. A* **2000**, *62*, 023202/1−7. (b) Larsson, M. O.; Hvelplund, P.; Larsen, M. C.; Shen, H.; Cederquist, H.; Schmidt, H. T. *Int. J. Mass Spectrom.* **1998**, *177*, 51–62.

0.8, 1.0, and 2.0 eV, and the irradiation time was 50, 80, and 150 ms. The ECD mass spectra obtained on the Thermo and Bruker FT-ICR instruments under comparable irradiation times and electron energies were nearly identical.

Calculations. Conformational Search. A recently developed conformational search engine[23] devised to deal with protonated peptides was used to scan the PESs of doubly protonated pentapeptides AHADL, AHDAL, and AAHAL. These calculations started with molecular dynamics (MD) simulations on the doubly charged species protonated at the N-terminal amino group and the His side-chain ring using the Insight II program (Biosym Technologies, San Diego, CA) in conjunction with the AMBER force field.[24] During the MD we used simulated annealing techniques to produce candidate structures for further refinement, applying full geometry optimization using the AMBER force field. The AMBER-optimized structures were analyzed by a conformer family search program developed in Heidelberg. This program groups optimized structures into families for which the most important characteristic torsion angles of the ion are similar. The most stable species in the families were then fully optimized at semiempirical (PM3) and Hartree−Fock (HF/3-21G) levels, where the conformer families were regenerated at each level. Typically, 15−20 lowest energy structures from the HF calculations were selected by the familial program[25] and considered for B3LYP/6-31+G(d,p) geometry re-optimization and single-point energy calculations. A modified approach was used for the conformational search of $(AAHAR + 2H)^{2+}$ ions. This relied on replica exchange[26] generation of several thousand conformers using the NAMD program[27a] and the CHARMM force field.[27b] The conformer geometries were re-optimized by the PM6 method,[28] and the structures were analyzed by their hydrogen-bonding patterns using a custom-made family search program. Conformers within 24 kJ mol^{-1} of the PM6 global energy minimum were re-optimized by B3LYP/6-31+G(d,p) and subjected to single-point energy calculations for energy ranking.

Quantum Chemistry Calculations. Standard ab initio and density functional theory (DFT) calculations were performed using the Gaussian 03 suite of programs.[29] Geometries were optimized with the hybrid B3LYP functional[30] using the 6-31+G(d,p) basis set. The optimized structures are presented in schemes and figures herein with the following atom color coding: turquoise, C; red, O; blue, N; and gray, H. Hydrogen bonds are indicated by light blue double arrows. Stationary points were characterized by harmonic frequency calculations to identify local energy minima (all real frequencies) and first-order saddle points (one imaginary frequency). Improved energies were obtained by single-point calculations using B3LYP and the Møller−Plesset perturbational theory[31] (second order, frozen core) with the larger 6-311++G(2d,p) basis set. For the pentapeptide ions under study (71−75 atoms), the basis set consisted of 1761−1896 primitive gaussians, and the MP2 calculations required >50 GB scratch space. Calculations on all open-shell species (radicals and cation-radicals) used the spin-unrestricted formalism. Spin contamination was quite modest and was treated by Schlegel's spin annihilation protocol.[32] The B3LYP and spin-projected MP2 (PMP2) energies were averaged to compensate for small errors inherent to both approximations according to the procedure reported previously.[33] Excited electronic states were calculated using time-dependent DFT[34] with the B3LYP functional and 6-311++G(2d,p) basis set. Charge and spin densities were calculated using natural population analysis[35] of B3LYP/6-311++G(2d,p) wave functions. Unimolecular rate constants were calculated using the RRKM theory[36] and employing a modified Hase's program.[37] The RRKM rate constants were obtained by direct count of quantum states at internal energies that were increased in 2 kJ mol^{-1} steps from the transition state up to 400 kJ mol^{-1} above the reactant. Rotations were treated adiabatically, and the calculated microscopic rate constants $k(E,J,K)$ were then Boltzmann-averaged over the thermal distribution of rotational states at 298 K.

Results

Doubly protonated peptides were produced by electrospray ionization and subjected to charge reduction under three different experimental conditions. In the first series of measurements carried out with AHDAL, AHADL, AAHAL, and AAHAL methyl ester, the doubly protonated peptides were accelerated to 100 keV, selected by mass, and partially discharged by glancing collisions with Cs atoms. The resulting spectra are referred to as electron-capture induced dissociations (ECID).[21] In a second series of measurements carried out with the entire set of peptides, electrospray-produced doubly charged ions were stored in a linear ion trap and discharged by ion−ion reactions with fluoranthene anion-radicals to provide electron-transfer dissociation (ETD) mass spectra. These two experiments substantially differ in the time scales for the interaction between the electron acceptor and donor and in the lifetimes of the charge-reduced intermediates and products, as will be discussed in more detail later. In a third series of experiments, also carried out with the entire set of peptides, electrospray-produced doubly charged ions were trapped in a Penning trap and allowed to recombine with free electrons to provide electron-capture dissociation (ECD) mass spectra. The results of these experiments are presented and discussed in the following section.

Electron-Induced Dissociations of Non-tryptic Peptide Ions. Electron-induced dissociations of the non-tryptic peptides are represented by the ECID, ETD, and ECD mass spectra of the doubly protonated AAHAL ion at m/z 241.6 (Figure 1a−c). The ECID and ETD spectra of doubly protonated AAHAL peptide ions were similar, showing a prominent charge-reduced ion at m/z 483 and fragments due to loss of H (m/z 482),

(22) Chamot-Rooke, J.; Malosse, C.; Frison, G.; Tureček, F. *J. Am. Soc. Mass Spectrom.* **2007**, *18*, 2146–2161.
(23) (a) Paizs, B.; Suhai, S. *J. Am. Soc. Mass Spectrom.* **2004**, *15*, 103–113. (b) Paizs, B.; Suhai, S.; Hargittai, B.; Hruby, V. J.; Somogyi, A. *Int. J. Mass Spectrom.* **2002**, *219*, 203–232. (c) Wyttenbach, T.; Paizs, B.; Barran, P.; Breci, L. A.; Liu, D.; Suhai, S.; Wysocki, V. H.; Bowers, M. T. *J. Am. Chem. Soc.* **2003**, *123*, 13768–13775. (d) Polfer, N. C.; Oomens, J.; Suhai, S.; Paizs, B. *J. Am. Chem. Soc.* **2007**, *129*, 5887–5897.
(24) Case, D. A.; et al. *AMBER 99*; University of California: San Francisco, 1999.
(25) (a) Bleiholder, C.; Osburn, S.; Williams, T. D.; Suhai, S.; Van Stipdonk, M.; Harrison, A. G.; Paizs, B. *J. Am. Chem. Soc.* **2008**, *130*, 17774–17789. (b) Paizs, B.; Suhai, S.; Hargittai, B.; Hruby, V. J.; Somogyi, A. *Int. J. Mass Spectrom.* **2002**, *219*, 203–232.
(26) Sugita, Y.; Okamoto, Y. *Chem. Phys. Lett.* **1999**, *314*, 141–151.
(27) (a) Phillips, J. C.; Braun, R.; Wang, W.; Gumbart, J.; Tajkhorshid, E.; Villa, E.; Chipot, C.; Skeel, R. D.; Kale, L.; Schulten, K. *J. Comput. Chem.* **2005**, *26*, 1781–1802. (b) MacKerell, A. D., Jr.; et al. *J. Phys. Chem. B* **1998**, *102*, 3586–3616.
(28) Stewart, J. J. P. *J. Mol. Model.* **2007**, *13*, 1173–1213.
(29) Frisch, M. J.; et al. *Gaussian 03*, Revision B.05; Gaussian, Inc.: Pittsburgh, PA, 2003.
(30) (a) Becke, A. D. *J. Chem. Phys.* **1993**, *98*, 1372–1377. (b) Becke, A. D. *J. Chem. Phys.* **1993**, *98*, 5648–5652. (c) Stephens, P. J.; Devlin, F. J.; Chabalowski, C. F.; Frisch, M. J. *J. Phys. Chem.* **1994**, *98*, 11623–11627.
(31) Møller, C.; Plesset, M. S. *Phys. Rev.* **1934**, *46*, 618–622.
(32) (a) Schlegel, H. B. *J. Chem. Phys.* **1986**, *84*, 4530–4534. (b) Mayer, I. *Adv. Quantum Chem.* **1980**, *12*, 189–262.
(33) Tureček, F. *J. Phys. Chem. A* **1998**, *102*, 4703–4713.
(34) Stratmann, R. E.; Scuseria, G. E.; Frisch, M. J. *J. Chem. Phys.* **1998**, *109*, 8218–8224.
(35) Reed, A. E.; Weinstock, R. B.; Weinhold, F. *J. Chem. Phys.* **1985**, *83*, 735.
(36) Gilbert, R. G.; Smith, S. C. *Theory of Unimolecular and Recombination Reactions*; Blackwell Scientific Publications: Oxford, 1990; pp 52−132.
(37) Zhu, L.; Hase, W. L. *Quantum Chemistry Program Exchange*; Indiana University: Bloomington, IN, 1994; Program No. QCPE 644.

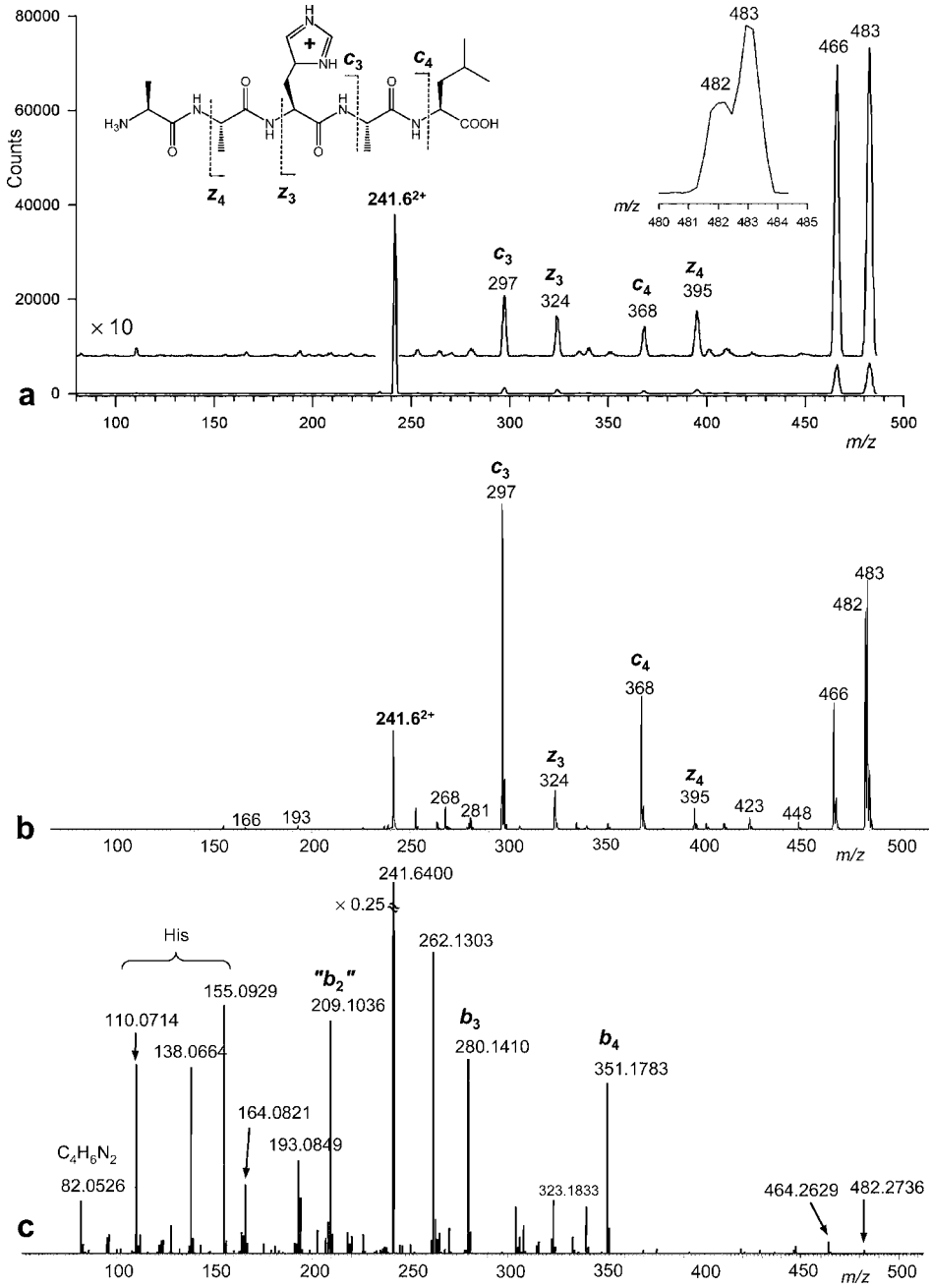

Figure 1. Tandem mass spectra of doubly protonated AAHAL peptide at *m*/*z* 241.6. (a) Electron-transfer induced dissociation spectrum at 100 keV, collisions with Cs. Inset shows the *m*/*z* 480−485 region measured at increased mass resolution. (b) Electron-transfer dissociation mass spectrum from 200-ms interaction with fluoranthene anions. (c) Electron-capture dissociation mass spectrum at 300-ms ion−electron interaction.

ammonia (*m*/*z* 466), and the sequence z_4 (*m*/*z* 395), z_3 (*m*/*z* 324), c_4 (*m*/*z* 368), and c_3 (*m*/*z* 297) ions, which all contained the His residue (Figure 1a,b). Thus, all four N−C_α bonds were cleaved upon electron transfer. The fragment peak assignments are corroborated by ECID and ETD spectra of AAHAL methyl ester (Figures S1 and S2, Supporting Information), which show 14 Da mass shifts for the C-terminal z_4 (*m*/*z* 409) and z_3 (*m*/*z* 338) ions but no shifts for the N-terminal c_3 and c_4 fragments. The relative intensities of the *c* and *z* fragment ions in the ETD spectrum of AAHAL and its methyl ester did not change upon extending the ion−ion interaction time from 100 to 200 ms and do not appear to be affected by depletion by secondary electron transfer from the fluoranthene anion.

The ECD spectrum of doubly protonated AAHAL ions (Figure 1c) dramatically differs from the ECID and ETD spectra in that the charge-reduced ion and the *c* and *z* fragments are absent or extremely weak. The major ion series corresponds to b_3 and b_4 ions at *m*/*z* 280 and 351, the internal "b_2" (AH/HA) ion at *m*/*z* 209, and His internal fragments at *m*/*z* 110, 138, and 155. The *b*-ion series is also prominent in the IRMPD spectrum of singly protonated AAHAL (*m*/*z* 482, Figure S3a, Supporting Information). The major formation of *b* ions in the ECD spectrum can be explained by electron-capture-induced loss of a hydrogen atom followed by charge-induced dissociation of the *m*/*z* 482 fragment ion.[9]

The electron-transfer mass spectra of ions from the other non-tryptic peptides, AHAAL, AHDAL, and AHADL, were quite analogous to the spectrum of the AAHAL ion. One-electron reduction with both Cs and fluoranthene anion-radical resulted in substantial charge-reduced ions (Figures S4−S6, Supporting

Table 1. Relative Intensities of Backbone *c* and *z* Fragment Ions in ETD and ECD Spectra

	relative intensity (%)[a,b]									
peptide	$(M + 2H)^{+\bullet}$	z_4	z_3	z_2	z_1	c_4	c_3	c_2	c_1	$\Sigma(c_i + z_i)$
AAHAL	16.8[c]	1.6	2.8	–	–	8.6	20.0	0.1	–	33.1
	–[c]	–	–	–	–	–	0.1	0.8	–	0.9
AAHAL-OMe	16.5	1.6	3.0	–	–	4.4	26.5	–	–	35.5
	–	–	–	–	–	–	0.1	0.6	–	0.7
AHAAL	14.5	5.8	0.1	–	–	12.9	6.8	11.0	–	36.6
	–	–	–	–	–	–	–	–	–	–
AHDAL	17.3	2.8	0.2	–	–	9.5	5.1	8.5	–	26.1
	–	–	–	–	–	–	0.1	0.6	–	0.7
AHADL	15.4	3.6	–	–	–	10.2	8.5	7.4	–	29.7
	–	–	–	–	–	–	–	0.6	–	0.6
AAAHK	24.7	2.0	10.2	7.5	–	10.9	–	–	–	30.6
	–	–	0.1	–	–	–	0.1	–	0.2	0.4
AAHAK	20.0	1.7	13.5	0.2	–	4.7	19.4	–	–	39.5
	–	–	–	1.6	–	–	0.3	–	–	1.9
AHAAK	22.9	5.3	9.4	–	–	8.0	7.3	8.7	–	38.7
	–	–	0.6	0.1	–	–	–	0.8	–	1.5
HAAAK	16.9	5.7	1.3	–	–	5.4	12.1	6.7	0.7	31.9
	–	0.2	0.4	0.3	–	–	–	0.5	1.0	2.4
AAAHR	24.3	2.7	5.9	3.3	5.1	6.8[d]	–	–	–	23.8
	–	0.3	–	0.1	5.0	0.6	–	–	–	6.0
AAHAR	26.3	1.8	6.6	6.4	3.5	2.4[d]	0.2	–	–	20.9
	–	0.2	–	3.6	1.2	0.2	–	0.1	–	5.3
AHAAR	23.5	4.8	11.6	2.4	4.1	1.3	0.1	–	–	24.3
	–	–	1.5	0.5	2.5	–	–	–	–	4.5
HAAAR	20.3	5.5	2.7	2.0	5.3	3.3	0.4	–	–	19.2
	–	0.3	0.3	0.6	1.9	–	–	–	–	3.1

[a] For the most abundant (^{12}C,^{14}N) isotopologue. [b] Relative to the sum of charge-reduced ion intensities. [c] Upper line values are from ETD spectra measured at 200-ms ion−ion interaction; lower line values are from ECD spectra measured at 300-ms ion−electron interaction. [d] Corrected for the contributions by ($^{13}C + {}^{15}N$) isotope satellites of the z_3 ion at *m*/*z* 368.

Information) and produced complete series of sequence *c* and *z* ions that all contained the histidine residue. In contrast, the ECD spectra showed no or weak *c*/*z* sequence ions and were dominated by fragments arising by loss of an H atom followed by backbone dissociations forming fragment ions of the *b* type.

The relative intensities of charge-reduced ions as well as *c* and *z* fragment ions in the ETD and ECD spectra are summarized in Table 1. The ETD data show that the peptide sequence in these histidine-containing ions had only a weak effect on the relative intensities of charge-reduced ions and the sum of *c* and *z* ion relative intensities. The *c*-type ions accounted for 84−89% of fragment ion intensities. The charging proton was retained in the His-containing fragments.

Electron-Induced Dissociations of Tryptic Peptide Ions. Electron-induced dissociations of the series of tryptic pentapeptides are represented by the ETD and ECD mass spectra of doubly protonated AAHAR (Figure 2a,b). The ETD spectrum (Figure 2a) shows a prominent charge-reduced ion at *m*/*z* 526, fragments by loss of H (*m*/*z* 525) and ammonia (*m*/*z* 509), and a complete series of sequence *z* ions containing the protonated arginine residue. In contrast, the ECD spectrum (Figure 2b) shows a dominant fragment at *m*/*z* 525 by loss of H, z_1 and z_2 cation-radical backbone fragments, and low-mass fragment ions originating from the arginine side chain ($C_3H_9N_3^{+\bullet}$ and $C_4H_{10}N_3^+$, Figure 2b).

The ETD and ECD spectra of the other tryptic pentapeptides followed a similar pattern (Table 1). The ETD spectra all showed intense charge-reduced ions and complete series of sequence *c* or *z* ions. The charge distribution between these two ion series depended on the nature of the basic residues. For Lys-terminated ions, z_1(K) and z_2(AK) fragment ions were weak or absent, whereas the complementary c_4 and c_3 His-containing ions were abundant in the ETD spectra. For Arg-terminated ions, the charging proton remained on the Arg-containing residues, forming complete *z* ion series. The ECD spectra of the Lys-terminated ions showed only minor *c* and *z* fragments (0.4−2.4% total) from dissociations occurring near the C or N peptide terminus. The ECD spectra of the Arg-terminated ions showed somewhat higher *c* and *z* ion relative intensities (3.1−6% total), which again originated from $N-C_\alpha$ bond cleavages near the C-terminal Arg residue.

Survivor Ion Dissociations. A conspicuous feature of the ECID and ETD spectra was the substantial relative intensities of charge-reduced $(M + 2H)^{+\bullet}$ ions for both non-tryptic and tryptic His-containing peptides. We utilized the MS^n capabilities of the linear ion trap to characterize the charge-reduced survivor ions in the ETD spectra of all peptides under study. The MS^3 collision-induced dissociation (CID) spectra of charge-reduced and mass-selected peptide ions showed some general features which are illustrated here by the spectra of $(AAHAL + 2H)^{+\bullet}$ (*m*/*z* 483, Figure 3a) and $(AAHAR + 2H)^{+\bullet}$ (*m*/*z* 526, Figure 3b), which are representative of the two sets of peptides. The ETD-CID-MS^3 spectra showed prominent fragment ions formed by elimination a $C_4H_6N_2$ (82 Da) neutral fragment[8,15] from the His side chain to give the *m*/*z* 401 and 444 fragment ions from AAHAL and AAHAR, respectively (Figure 3). Loss of the 82 Da neutral fragment dominated the ETD-CID-MS^3 spectra of charge-reduced ions from all His-containing peptide ions we studied. The ETD-CID-MS^3 spectra further displayed sequence b_n ($n = 3$, 4) and y_n ($n = 3$ from AAHAL and $n = 1$ for AAHAR) ions carrying the basic residues. The *b* ions were accompanied by ions containing an additional hydrogen atom, which are denoted as $b_n + 1$ ions. In contrast, the *c* and *z* sequence fragment ions were either very weak or completely missing. The stark differences between the nature of the fragments in the ETD spectra and those in the CID spectra of

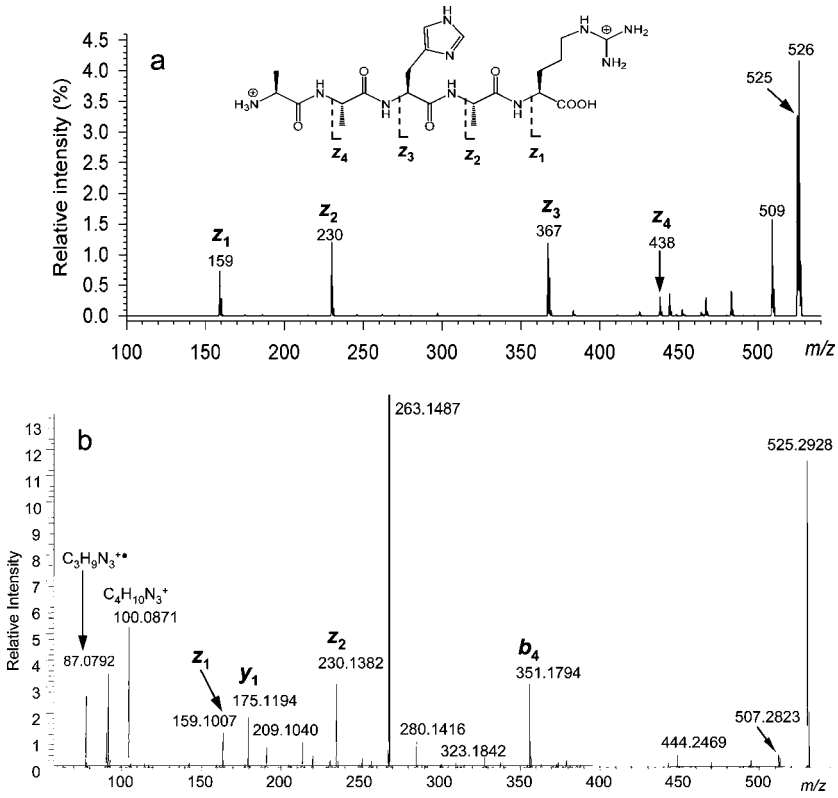

Figure 2. Tandem mass spectra of doubly protonated AAHAR peptide at *m*/*z* 263. (a) Electron-transfer dissociation mass spectrum from 200-ms interaction with fluoranthene anions. (b) Electron-capture dissociation mass spectrum at 300-ms ion−electron interaction.

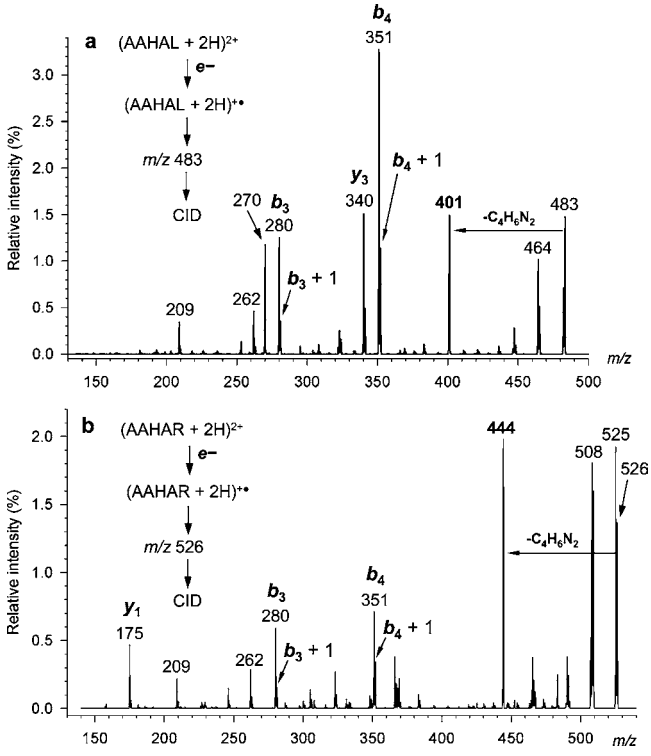

Figure 3. ETD-CID-MS^3 mass spectra of charge-reduced ions from (a) AAHAL at *m*/*z* 483 and (b) AAHAR at *m*/*z* 526.

the charge-reduced ions strongly indicated that the latter did not retain the original peptide structure nor were they noncovalent ion−molecule complexes of the incipient *c* and *z* fragments.[38]

Discussion

The experimental data revealed two major effects. The most unusual one was the dramatic difference between the dissociations of peptide ions induced by free electron attachment and those induced by electron transfer. The other effect was the difference between the dissociations induced by electron transfer and the CID of long-lived charge-reduced ions. To shed more light on these effects, we employed ab initio and DFT calculations to address some key questions relevant to electron transfer and capture. The calculations addressed (i) precursor cation structures, (ii) electron-transfer and -capture energetics, (iii) cation-radical geometries and electronic structure, and (iv) N−C_α backbone dissociations. Here we discuss data for AAHAL and AAHAR as the respective representatives of the non-tryptic and tryptic peptides. Details for several other cations, cation-radicals, and their dissociation pathways are compiled in the Supporting Information.

Precursor Cation Structures. Electron attachment to peptide ions is thought to depend on the protonation sites and ion secondary structure, which are the principal structural characteristics of the reactant ions. Protonation in the non-tryptic peptides was presumed to occur in the His ring and at the N-terminus, which are the most basic sites in these peptides. Protonation in the tryptic-type peptides was presumed to occur in the His ring and at the C-terminal Lys or Arg.[20] The other potential protonation sites, such as the amide oxygens,[39] are less basic according to both theory[40] and experiment. For

(38) (a) Xia, Y.; Han, H.; McLuckey, S. A. *Anal. Chem.* **2008**, *80*, 1111–1117. (b) Han, H.; Xia, Y.; McLuckey, S. A. *J. Proteome Res.* **2007**, *6*, 3062–3069. (c) Savitski, M. M.; Kjeldsen, F.; Nielsen, M. L.; Zubarev, R. A. *J. Am. Soc. Mass Spectrom.* **2007**, *18*, 113–121.

Scheme 1

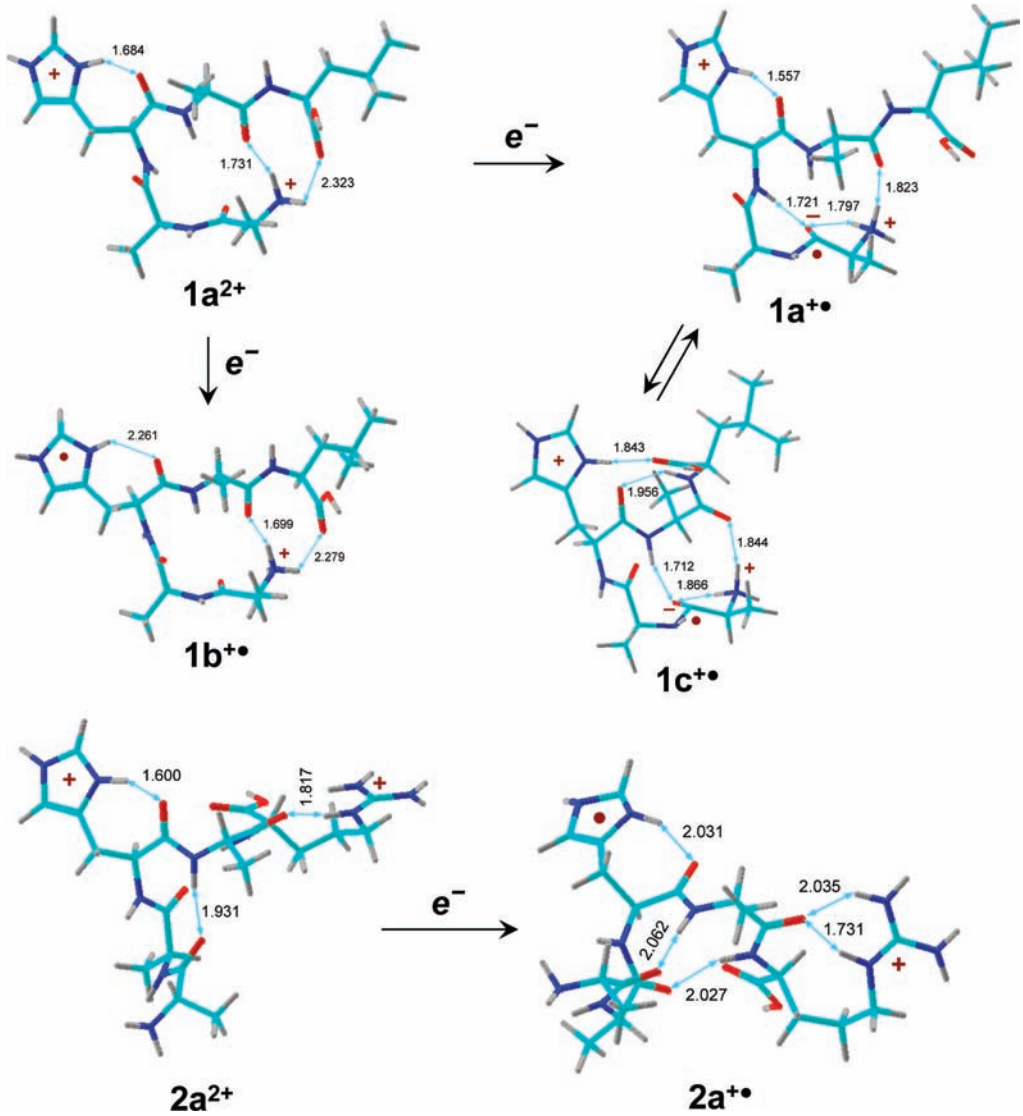

example, double protonation did not occur in histidine-containing non-tryptic pentapeptides in which the N-terminus was blocked.

Doubly protonated AAHAL was found to prefer the conformation shown in Scheme 1 ($\mathbf{1a}^{2+}$), which was the global energy and free energy minimum according to B3-MP2 calculations and was likely to be formed by electrospray ionization.[41] Conformer $\mathbf{1a}^{2+}$ has the N-terminal ammonium hydrogen-bonded to the C-terminal carboxyl and the Ala_4 amide carbonyl. The relative energies of other low-energy conformers ($\mathbf{1b}^{2+}-\mathbf{1d}^{2+}$) are given in Table S1 (Supporting Information). Doubly protonated AAHAR preferred structure $\mathbf{2a}^{2+}$ as the global energy and free energy minimum according to both B3LYP and MP2. Structure $\mathbf{2a}^{2+}$ has the protonated Arg side chain internally solvated by the Ala_4 amide carbonyl, and the protonated His side chain is hydrogen-bonded to the His amide carbonyl (Scheme 1). Other ion conformers were less stable. The relative energies of low-energy conformers $\mathbf{2b}^{2+}-\mathbf{2d}^{2+}$ are collected in Table S1.

Exhaustive conformational searches were also carried out for doubly protonated AHDAL ($\mathbf{3a}^{2+}-\mathbf{3d}^{2+}$) and AHADL ($\mathbf{4a}^{2+}-\mathbf{4d}^{2+}$) sequences. The relative energies of the most stable ion conformers are given in Table S1. Their optimized structures are shown in Scheme S1 (Supporting Information) and given in the Cartesian coordinate format in Tables S2−S13 (Supporting Information).

Electron Capture and Transfer Energetics. Attachment of a free electron to a gas-phase ion is a highly exothermic process which can be characterized by the ion adiabatic recombination energy (RE_a). These were calculated to range between 4.9 and 5.5 eV for the peptide dications in question (Table 2) and indicated substantial excitation in the cation-radicals formed by electron capture. By comparison, an excitation of 5 eV in the cation-radical ($\mathbf{1a}^{+\bullet}$) formed by electron recombination with $\mathbf{1a}^{2+}$ is equivalent to the ion's ro-vibrational enthalpy at an 850 K thermal equilibrium.

(39) (a) Wu, R.; McMahon, T. B. *J. Phys. Chem. B* **2009**, *113*, 8767–8775. (b) Wu, R.; McMahon, T. B. *ChemPhysChem* **2008**, *9*, 2826–2835. (c) Wu, R.; McMahon, T. B. *J. Am. Chem. Soc.* **2007**, *129*, 11312–11313.

(40) Turecek, F.; Panja, S.; Wyer, J. A.; Ehlerding, A.; Zettergren, H.; Nielsen, S. B.; Hvelplund, P.; Bythell, B.; Paizs, B. *J. Am. Chem. Soc.* **2009**, *131*, 16472–16487.

(41) Ion mobility measurements by Dr. Iain Campuzano (private communication) gave the collisional cross section of $(AAHAL + 2H)^{2+}$ as 167.8 $Å^2$, in excellent agreement with the calculated cross section for structure $\mathbf{1a}^{2+}$ (164.7 $Å^2$).

Table 2. Ion Recombination Energies

reaction	recombination energy[a] B3LYP 6-31+G(d,p)	B3LYP 6-311++G(2d,p)	PMP2 6-311++G(2d,p)	B3-PMP2 6-311++G(2d,p)
$\mathbf{1a}^{2+} \rightarrow \mathbf{1a}^{+\bullet}$	5.33	5.32 (4.91)[b]	5.10 (4.00)[b]	5.21 (4.45)[b]
$\mathbf{1a}^{2+} \rightarrow \mathbf{1b}^{+\bullet}$	5.27	5.32	4.94	5.13
$\mathbf{1b}^{2+} \rightarrow \mathbf{1b}^{+\bullet}$	5.60	5.64	5.30	5.47
$\mathbf{1c}^{2+} \rightarrow \mathbf{1c}^{+\bullet}$	5.42	5.42 (5.05)[b]	5.18 (3.48)[b]	5.30 (4.26)[b]
$\mathbf{2a}^{2+} \rightarrow \mathbf{2a}^{+\bullet}$	5.08	5.13 (4.51)[b]	4.74 (3.47)[b]	4.97 (4.00)[b]
$\mathbf{3a}^{2+} \rightarrow \mathbf{3b}^{+\bullet}$	5.53	5.57	5.23	5.40
$\mathbf{3a}^{2+} \rightarrow \mathbf{3c}^{+\bullet}$	5.65	5.64 (5.10)[b]	5.42 (3.79)[b]	5.53 (4.49)[b]
$\mathbf{4a}^{2+} \rightarrow \mathbf{4a}^{+\bullet}$	5.41	5.47 (4.95)[b]	5.12 (4.08)[b]	5.29 (4.52)[b]
$\mathbf{4b}^{2+} \rightarrow \mathbf{4b}^{+\bullet}$	5.60	5.63	5.30	5.47

[a] In units of electronvolts. Adiabatic recombination energies include zero-point corrections. [b] Vertical recombination energies without zero-point corrections.

In contrast to ECD, the excitation imparted upon collisional electron transfer to a fast-moving ion as used in ECID is typically characterized by the energy balance between the ion vertical recombination energy, the donor vertical ionization energy (RE_v), and the term for the repulsion potential between the charged products (eq 1), where σ is the cross section for collisional electron transfer in Å^2 (10^{-16} cm^2).

$$\Delta E\ (\mathrm{eV}) = \mathrm{RE_v(ion)} - \left[\mathrm{IE(Cs)} + \frac{25.52}{\sqrt{\sigma}}\right] \qquad (1)$$

Hence, for cross sections of 10^2-10^3 Å^2, $RE_v = 4.5$ eV (Table 2), and IE(Cs) = 3.894 eV, one obtains negative ΔE values, indicating that the electron transfer is slightly endothermic. Under such conditions of endothermic electron transfer, the mean energy in the charge-reduced product $\langle E \rangle$ can be approximated[42] by the sum of the precursor ion ro-vibrational energy (77 kJ mol^{-1} for $\mathbf{1a}^{2+}$ at 298 K) and the Franck−Condon energy in vertical electron transfer (0.59 eV, 56 kJ mol^{-1}) to give $\langle E \rangle \approx 133$ kJ mol^{-1} (1.4 eV) for $\mathbf{1a}^{+\bullet}$ and likewise for the other peptide cation-radicals.

Collisional electron transfer in ETD can be characterized by the energy balance between the ion adiabatic recombination energy, the fluoranthene electron affinity, and the vibronic excitation energy in the departing neutral fluoranthene molecule (eq 2).

$$\Delta E\ (\mathrm{eV}) = \mathrm{RE_a(ion)} - [\mathrm{EA(anion)} + \Delta E_{\mathrm{exc}}(\mathrm{neutral})] \qquad (2)$$

The electron affinity of fluoranthene has been estimated at 0.63 eV,[43] and the singlet excitation energies are 3.06, 3.45, 3.83, and 4.32 eV for the S_1-S_4 states.[44] When combined with the peptide ion adiabatic recombination energy, e.g., $RE_a = 5.13$ eV for $\mathbf{1a}^{2+}$ (Table 2), this gives $\Delta E = 4.5$, 1.44, 1.05, 0.67, and 0.18 eV in charge-reduced ions for fluoranthene molecules formed in the S_0-S_4 electronic states. Hence, a range of excitation energies can be expected in ETD that depend on *the electronic state of the departing fluoranthene molecule*. The latter is likely to depend on the transition probabilities for the crossing of PESs[45] corresponding to the ground state of the peptide dication and fluoranthene anion reactants and the charge-reduced ion and fluoranthene singlet-state products. The excited states of the fluoranthene molecules can potentially be probed by detecting fluorescence emission at 455 nm[44b] from the ion−ion reaction.[46] It should be noted that electron transfer forming neutral fluoranthene molecules in the S_1 and S_2 states is energetically similar to fast collisional electron transfer from Cs atoms (vide supra) and may explain the similarity of dissociations observed in the ECID and ETD mass spectra.

Cation-Radical Structures. Electron attachment to peptide dications dramatically changes the intramolecular interactions in the charge-reduced cation-radicals. Major changes occur in the bond lengths, angles, and dihedrals of the groups affected by electron attachment which result in Franck−Condon effects in vertical electron transfer. Another major change is due to the lack of Coulomb repulsion in the cation-radicals, which is one of the dominant interactions in the dications.[47] Finally, the reduced functional groups develop intramolecular hydrogen-bonding arrangements which are distinctly different from those in the charged groups.[16]

Vertical electron attachment to $\mathbf{1a}^{2+}$ was calculated to produce a π^* state in which most of the unpaired electron density was rather extensively delocalized over the C-terminal carboxyl (45%), His ring (37%), and Ala_4 amide (15%). The positive charge is carried by the His ring (0.62) and the N-terminal ammonium group (0.6). This is consistent with the analysis of the six lowest electronic states of vertically reduced $\mathbf{1a}^{2+}$, which indicate extensive delocalization of electron density among the amide, carboxyl, and His ring π^* systems (Figure 4). For example, the **X** and **A** states are nearly degenerate ($\Delta E = 0.02$ eV), differing in the orbital phases of the His π^* system relative to those at the C-terminal carboxyl, Ala_1, and Ala_4 amide. The **B** state ($\Delta E = 0.17$ eV) is a combination of Ala_1 and Leu carbonyl π^* orbitals, the **C** state ($\Delta E = 0.27$ eV) involves the Ala_2 and Ala_4 amide π^* orbitals, the **D** state ($\Delta E = 0.42$ eV) involves the Ala_2, Ala_4, and C-terminal carboxyl π^* orbitals, and the **E** state ($\Delta E = 0.52$ eV) gets a main contribution from the Ala_1 and Ala_2 amide π^* orbitals. Hence, these six low-lying electronic states encompass electron distribution that is requisite for all major dissociations observed in the ECID and ETD mass spectra.

Geometry relaxation in charge-reduced $\mathbf{1a}^{2+}$ led to cation-radicals $\mathbf{1a}^{+\bullet}$ and $\mathbf{1b}^{+\bullet}$, which were local energy minima (Scheme 1). The lowest-energy structure, $\mathbf{1a}^{+\bullet}$, is a zwitterion. This unusual finding is corroborated by the charge distribution in $\mathbf{1a}^{+\bullet}$, which showed that the positive charge was carried by the protonated His ring (0.90), which had a typical planar geometry, and by the N-terminal ammonium group (0.59). These moieties displayed negligible spin density and showed intramolecular hydrogen bonds which were typical of analogous charged groups in peptide ions.[16,47] Most of the spin density was actually localized in the Ala_1 amide (88%), which also carried a

(42) Tureček, F. *Int. J. Mass Spectrom.* **2003**, *227*, 327–338.
(43) Chaudhuri, J.; Jagur-Grodzinski, J.; Szwarc, M. *J. Phys. Chem.* **1967**, *71*, 3063–3065.
(44) (a) Maddams, W. F.; Schnurmann, R. *J. Chem. Phys.* **1951**, *19*, 973–974. (b) Michl, J. *J. Mol. Spectrosc.* **1969**, *30*, 66–76. (c) Ruth, A. A.; Wick, M. T. *Chem. Phys. Lett.* **1997**, *266*, 206–216.
(45) (a) Gunawardena, H. P.; He, M.; Chrisman, P. A.; Pitteri, S. J.; Hogan, J. M.; Hodges, B. D. M.; McLuckey, S. A. *J. Am. Chem. Soc.* **2005**, *127*, 12627–12639. (b) Xia, Y.; Chrisman, P. A.; Pitteri, S. J.; Erickson, D. E.; McLuckey, S. A. *J. Am. Chem. Soc.* **2006**, *128*, 11792–11798.
(46) (a) Poon, C.; Lin, Y.; Mayer, P. M. *J. Phys. Chem. A* **2008**, *112*, 7761−7767. *J. Am. Chem. Soc.* **2008**, *130*, 8818−8833. (b) Poon, C.; Mayer, P. M. *J. Phys. Chem. A* **2007**, *111*, 777–782. (c) Chingin, K.; Chen, H.; Gamez, G.; Zenobi, R. *J. Am. Soc. Mass Spectrom.* **2009**, *20*, 1947–1963.
(47) Tureček, F.; Chen, X.; Hao, C. *J. Am. Chem. Soc.* **2008**, *130*, 8818–8833.

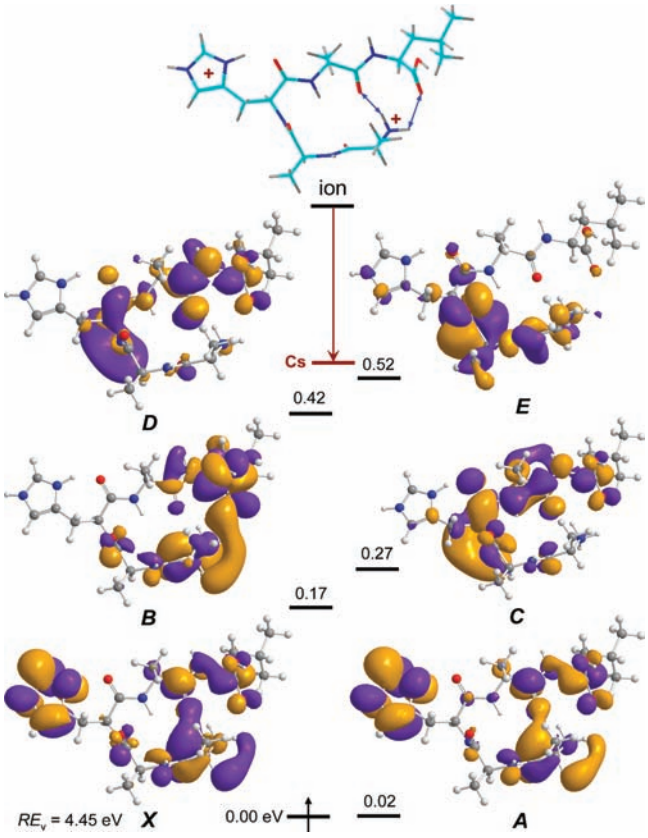

Figure 4. Electronic state diagram for vertical electron attachment to cation $\mathbf{1}^{2+}$. The excitation energies (eV) are from TD-B3LYP/6-311++G(2d,p) calculations.

substantial negative charge (−0.83). The Ala_1 carbonyl in $\mathbf{1a}^{+\bullet}$ was puckered and had a long C−O bond (1.324 Å), whereby the oxygen atom developed a strong hydrogen bond to the Ala_2 amide N−H (1.721 Å, Scheme 1).

Structure $\mathbf{1b}^{+\bullet}$ arose by histidine ring puckering in $\mathbf{1a}^{+\bullet}$, accompanied by an electron and hydrogen bond reorganization, which resulted in a slight increase in energy (Table 3). Structure $\mathbf{1b}^{+\bullet}$ is a typical His radical,[16,17] which has most of the unpaired electron density in the His ring while the charge is carried by the N-terminal ammonium.

A slight conformational change in $\mathbf{1a}^{+\bullet}$ led to cation-radical $\mathbf{1c}^{+\bullet}$, which was another zwitterionic conformer. This was indicated by the optimized geometry, which showed a substantially pyramidized Ala_1 amide group with a long C−O bond at 1.324 Å and strong hydrogen bonds to the His amide proton and the N-terminal ammonium (Scheme 1). The Ala_1 amide group carried 87% of the spin density and a −0.81 negative charge. The planar His ring in $\mathbf{1c}^{+\bullet}$ carried a +0.88 charge and practically no spin density. The N-terminal ammonium carries a 0.58 charge and 2% of spin density. Structure $\mathbf{1c}^{+\bullet}$ was 4 kJ mol^{-1} more stable than $\mathbf{1a}^{+\bullet}$ by combined B3LYP and MP2 calculations (Table 3).

Vertical electron attachment to ion $\mathbf{2a}^{2+}$ can lead to any of the low-lying electronic states in the charge-reduced ion $\mathbf{2a}^{+\bullet}$. These electronic states were closely spaced, so that the first 12 states were within 1 eV of the ground state (Figure S7, Supporting Information) and were quite analogous to those of $\mathbf{1a}^{+\bullet}$. The general feature of the electronic states in vertically formed $\mathbf{2a}^{+\bullet}$ was that the electron density was delocalized among the π^* systems of the His ring, Arg guanidinium, amide, and carboxyl groups. Geometry relaxation led to a His radical ($\mathbf{2a}^{+\bullet}$) that showed a typical puckered imidazolium ring (Scheme 1).

Table 3. Cation-Radical Relative Energies

	relative energy[a]			
	B3LYP		PMP2	B3-PMP2
reaction	6-31+ G(d,p)	6-311++ G(2d,p)	6-311++ G(2d,p)	6-311++ G(2d,p)
$\mathbf{1a}^{+\bullet} \rightarrow \mathbf{1b}^{+\bullet}$	5	0.0	16	8
$\mathbf{1a}^{+\bullet} \rightarrow \mathbf{1c}^{+\bullet}$	4	5	−14	−4
$\mathbf{1a}^{+\bullet} \rightarrow \mathbf{1d}^{+\bullet}$	−31	−32	−26	−29
$\mathbf{1a}^{+\bullet} \rightarrow \mathbf{TS1}$	−5	−4	−5	−4
$\mathbf{1d}^{+\bullet} \rightarrow \mathbf{TS2}$	52	49	68	59
$\mathbf{1a}^{+\bullet} \rightarrow \mathbf{TS3}$	46	43	63	53
$\mathbf{1a}^{+\bullet} \rightarrow \mathbf{1e}^{+\bullet}$	−8	−9	3	−3
$\mathbf{1e}^{+\bullet} \rightarrow \mathbf{TS4}$	40	38	52	45
$\mathbf{1a}^{+\bullet} \rightarrow z_4^{+\bullet} + c_1$	−27	−36	31	−2
$\mathbf{1a}^{+\bullet} \rightarrow z_3^{+\bullet} + c_2$	3	−6	68	31
$\mathbf{1a}^{+\bullet} \rightarrow c_4^{+} + z_1^{\bullet}$	−44	−54	1	−24
$\mathbf{1a}^{+\bullet} \rightarrow c_3^{+} + z_2^{\bullet}$	−89	−97	−27	−63
$\mathbf{1a}^{+\bullet} \rightarrow \mathbf{1f}^{+\bullet}$	−31	−32	−33	−33
$\mathbf{1a}^{+\bullet} \rightarrow \mathbf{1g}^{+\bullet}$	−17	−20	−20	−20
$\mathbf{1g}^{+\bullet} \rightarrow \mathbf{TS5}$	−4	2	−9	−4
$\mathbf{1f}^{+\bullet} \rightarrow \mathbf{TS6}$	29	27	39	33
$\mathbf{1f}^{+\bullet} \rightarrow \mathbf{1h}^{+\bullet}$	−59	−64	−36	−50
$\mathbf{1f}^{+\bullet} \rightarrow c_3^{+} + z_2^{\bullet}$	−57	−66	6	−30
$\mathbf{1a}^{+\bullet} \rightarrow \mathbf{1i}^{+\bullet}$	−40	−39	−38	−38
$\mathbf{1i}^{+\bullet} \rightarrow \mathbf{TS7}$	36	32	50	41
$\mathbf{1i}^{+\bullet} \rightarrow \mathbf{TS8}$	40	40	44	42
$\mathbf{1i}^{+\bullet} \rightarrow \mathbf{1k}^{+\bullet}$	−51	−54	−41	−48
$\mathbf{1k}^{+\bullet} \rightarrow c_4^{+} + z_1^{\bullet}$	47	44	80	62
$\mathbf{1i}^{+\bullet} \rightarrow \mathbf{1j}^{+\bullet}$	−20	−27	2	−12
$\mathbf{1h}^{+\bullet} \rightarrow \mathbf{1j}^{+\bullet}$	16	15	48	32
$\mathbf{1b}^{+\bullet} \rightarrow \mathbf{1m}^{+\bullet}$	−115	−115	−100	−107
$\mathbf{1a}^{+\bullet} \rightarrow \mathbf{TS9}$	2	2	12	7
$\mathbf{1a}^{+\bullet} \rightarrow \mathbf{TS10}$	84	77	85	81
$\mathbf{2c}^{+\bullet} \rightarrow \mathbf{2d}^{+\bullet}$	−4	−4	3	−1
$\mathbf{2c}^{+\bullet} \rightarrow \mathbf{TS11}$	−9	−9	−5	−7
$\mathbf{3a}^{+\bullet} \rightarrow \mathbf{3b}^{+\bullet}$	12	7	17	12
$\mathbf{3b}^{+\bullet} \rightarrow \mathbf{3c}^{+\bullet}$	−114	−111	−119	−115

[a] In units of kJ mol^{-1}. Including B3LYP/6-31+G(d,p) zero-point energies and referring to 0 K.

N−C_α Backbone Dissociations. The N−C_α backbone dissociations were studied in detail for AAHAL cation-radicals where they led to the *c* and *z* fragment ions. Calculated dissociation and transition-state (TS) energies are compiled in Table 3. The N−C_α bonds for which TSs were located, the fragments formed, and their relative intensities in ECID and ETD spectra are summarized in Scheme 2. Detailed structures of all intermediates and TSs and description of the dissociation pathways are given in Schemes S2−S6 in the Supporting Information.

Transition states **TS2**−**TS4** and **TS6**−**TS8** are relevant for the dissociations of the four N−C_α bonds in AAHAL cation-radicals. **TS2** and **TS3** (Scheme S2) pertain to two different modes of Ala_1-N−C_α-Ala_2 bond cleavage, starting from an Ala_1 aminoketyl intermediate ($\mathbf{1d}^{+\bullet}$) and a zwitterion ($\mathbf{1a}^{+\bullet}$), respectively, and leading to the $z_4^{+\bullet}$ fragment ion. **TS4** pertains to an Ala_2-N−C_α-His bond cleavage starting from an Ala_2 aminoketyl radical ($\mathbf{1e}^{+\bullet}$) and leading to the $z_3^{+\bullet}$ fragment ion (Scheme S3). **TS6** (Scheme S4) and **TS7** (Scheme S5) refer to two different modes of His-N−C_α-Ala_4 bond cleavage, one starting from a His aminoketyl radical ($\mathbf{1f}^{+\bullet}$) and the other from an Ala_4 aminoketyl radical ($\mathbf{1i}^{+\bullet}$), both leading to the c_3^{+} fragment ion. Finally, **TS8** refers to an Ala_4-N−C_α-Leu bond cleavage starting from $\mathbf{1i}^{+\bullet}$ and leading to the c_4^{+} fragment ion (Scheme S6). We have calculated the pertinent RRKM rate constants for these

Scheme 2

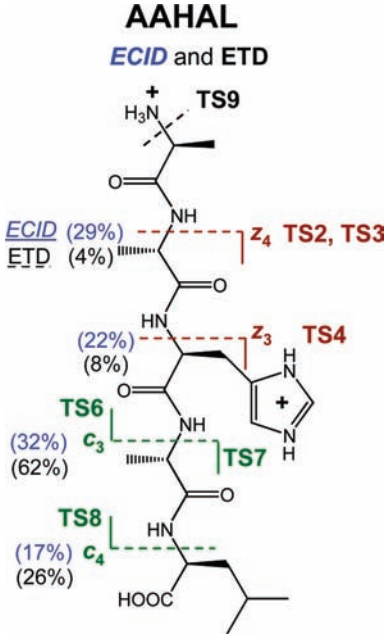

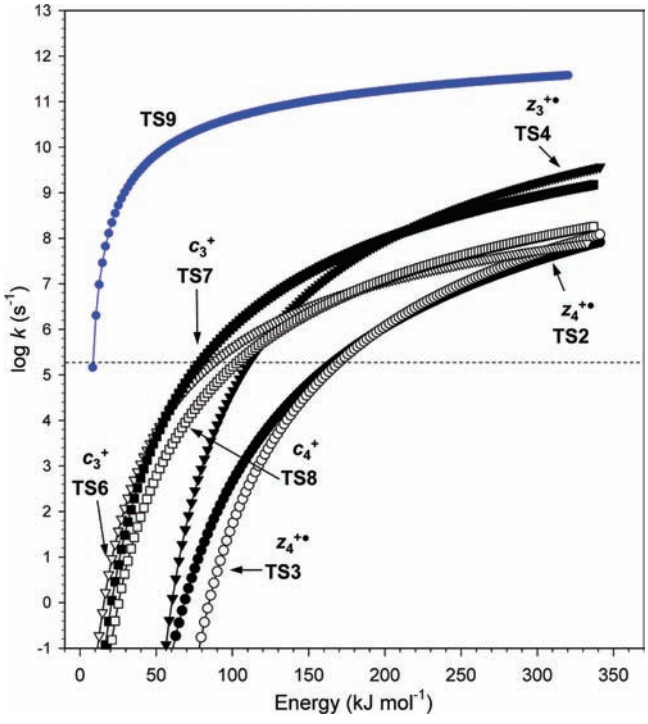

Figure 5. RRKM rate constants (log k, s^{-1}) for dissociations of (AAHAL + 2H)$^{+\bullet}$ cation-radicals: ●, formation of $z_4^{+\bullet}$ through **TS2**; ○, formation of $z_4^{+\bullet}$ through **TS3**; ▼, formation of $z_3^{+\bullet}$ through **TS4**; ▽, formation of c_3^+ through **TS6**; ■, formation of c_3^+ through **TS7**; □, formation of c_4^+ through **TS8**. Blue solid circles indicate loss of ammonia through **TS9**. The horizontal dashed line was drawn at log k = 5.30, corresponding to dissociations occurring on the ECID experimental time scale of 5 μs.

six dissociations, which are plotted as log k (s^{-1}) on a common energy scale referring to **1a**$^{+\bullet}$ (Figure 5). The plots in Figure 5 indicate that dissociations through **TS4**, **TS6**, **TS7**, and **TS8** can occur on the time scale of the ECID measurements (~5 μs) at the vibrational excitation due to vertical electron transfer (~133 kJ mol^{-1}, vide supra). In contrast, formation of $z_4^{+\bullet}$ through **TS2** and **TS3** is predicted by RRKM to be too slow within the same energy range and would require excitation on the order of ~170 kJ mol^{-1} to be kinetically feasible. Much less stringent kinetic constrains apply to ETD, which occurs on a longer time scale (>100 ms) and, according to our RRKM analysis, allows the dissociations to occur at internal energies ≥100 kJ mol^{-1}.

The RRKM rate constants allow one to estimate the energy-dependent branching ratios for the c and z ion formation (Figure S9, Supporting Information). The branching ratios show a qualitative agreement with the ETD data in that the formation of the c_3 fragment is preferred when proceeding through **TS6** at low internal energies (10−50 kJ mol^{-1}) and through **TS7** at intermediate internal energies (50−210 kJ mol^{-1}). However, quantitative agreement is less satisfactory, as the RRKM data underestimate the formation of the c_4 (<10%) and z_4 (~1%) fragments and predict efficient formation of the z_3 fragments only at high internal energies (>210 kJ mol^{-1}).

A more serious factor that complicates the kinetic analysis of backbone dissociations is the competing loss of ammonia from **1a**$^{+\bullet}$. This dissociation has a low activation energy in **TS9** (7 kJ mol^{-1}, Table 3), is fast according to RRKM calculations (Figure 5), and can deplete the population of **1a**$^{+\bullet}$, thus preventing backbone dissociations starting from **1a**$^{+\bullet}$. The formation of $z_4^{+\bullet}$ fragments depends on the competition between ammonia loss and isomerization through **TS1** to form intermediate **1d**$^{+\bullet}$, which is the reactant for subsequent N−C$_\alpha$ bond cleavage through **TS2** (Scheme S2). However, Figure 5 indicates that the loss of ammonia would outcompete an N−C$_\alpha$ bond dissociation proceeding through **TS3** from the same reactant (**1a**$^{+\bullet}$).

Electron Capture and Transfer Lead to Different Electronic States. The dramatic differences in the dissociations induced by electron transfer on one hand and capture of free electron on the other are unprecedented and point to different electronic states of peptide cation-radicals which are accessed in these processes. Therefore, the discussion must first address the electronic states. The finding in the present work that zwitterionic peptide cation-radicals such as **1a**$^{+\bullet}$, **1b**$^{+\bullet}$, and **3a**$^{+\bullet}$ exist as low-energy local minima is of fundamental importance for the interpretation of electron-based peptide ion dissociations. Previous mechanistic models included in the scheme developed by researchers in Utah and Washington[48,49] of electron-based peptide dissociations dealt with small amide or dipeptide systems and considered zwitterionic amide π^* states as excited electronic states pertinent to short-lived intermediates.[47] The present computational analysis indicates that amide π^* states in larger peptides can receive substantial stabilization through intramolecular hydrogen-bonding and Coulomb attraction between the carbonyl anion-radical and a proximate protonated group so that they represent low-lying or even *ground electronic states*. PESs of such ground states can be investigated to provide local energy minima for reactive intermediates and TS energies for isomerizations and dissociations.

(48) Syrstad, E. A.; Tureček, F. *J. Am. Soc. Mass Spectrom.* **2005**, *16*, 208–224.
(49) (a) Sobczyk, M.; Anusiewicz, I.; Berdys-Kochanska, J.; Sawicka, A.; Skurski, P.; Simons, J. *J. Phys. Chem. A* **2005**, *109*, 250–258. (b) Anusiewicz, I.; Berdys-Kochanska, J.; Simons, J. *J. Phys. Chem. A* **2005**, *109*, 5801–5813. (c) Anusiewicz, I.; Berdys-Kochanska, J.; Skurski, P.; Simons, J. *J. Phys. Chem. A* **2006**, *110*, 1261–1266. (d) Sobczyk, M.; Simons, J. *Int. J. Mass Spectrom.* **2006**, *253*, 274–280. (e) Sobczyk, M.; Simons, J. *J. Phys. Chem. B* **2006**, *110*, 7519–7527. (f) Skurski, P.; Sobczyk, M.; Jakowski, J.; Simons, J. *Int. J. Mass Spectrom.* **2007**, *265*, 197–212. (g) Sobczyk, M.; Neff, D.; Simons, J. *Int. J. Mass Spectrom.* **2008**, *269*, 149–164.

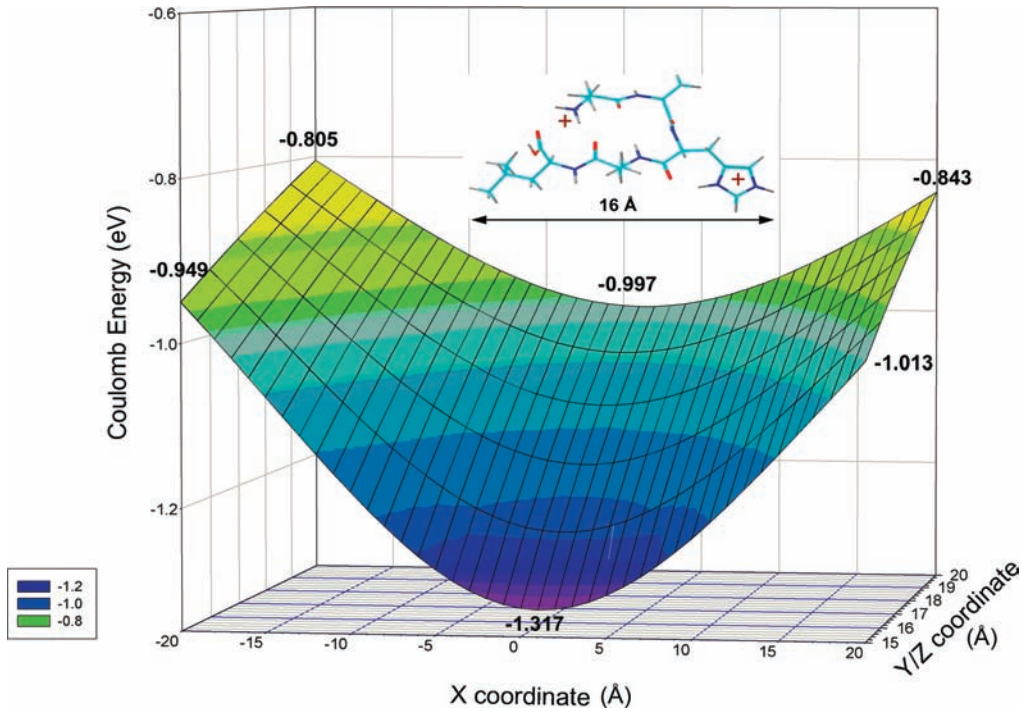

Figure 6. Electrostatic field around ion $\mathbf{1}^{2+}$. The ion is oriented along the *x* axis as shown, and the *y* and *z* coordinates are kept equal at 15−20 Å.

Regarding dissociations, the pentapeptides under study show a similar behavior upon electron transfer under experimental conditions that differ in the electron-transfer energetics and intermediate charge-reduced ion lifetimes. Cleavages of all four N−C_α backbone bonds, loss of H atoms, and elimination of ammonia are observed to occur on a time scale ranging from 10^{-6} s in ECID to 10^{-1} s in ETD. RRKM calculations for charge-reduced $(AAHAL + 2H)^{+\bullet}$ ions indicate that these dissociations probably do not occur competitively on the same PES but rather involve reactants formed from different electronic states of the charge-reduced intermediates. For example, the **X** state of relaxed $\mathbf{1a}^{+\bullet}$ is calculated to be dynamically unstable with respect to an exothermic isomerization through **TS1** to the aminoketyl cation-radical $\mathbf{1d}^{+\bullet}$, which is expected to steer the dissociation into the channel through **TS2** for the formation of the $z_4^{+\bullet}$ ion (Scheme S2). Although a reverse migration ($\mathbf{1d}^{+\bullet} \rightarrow \mathbf{1a}^{+\bullet}$) through **TS1** is kinetically feasible, the population of thus re-formed $\mathbf{1a}^{+\bullet}$ is too low to allow for an efficient branching to proton-transfer isomerizations forming $\mathbf{1e}^{+\bullet}$ and $\mathbf{1i}^{+\bullet}$, which are the precursors for the $z_3^{+\bullet}$, c_3^+, and c_4^+ fragment ions. It appears more plausible that aminoketyl radicals $\mathbf{1e}^{+\bullet}$ and $\mathbf{1i}^{+\bullet}$ are produced by proton transfer occurring in the low-lying **B**, **C**, and **D** states of charge-reduced $\mathbf{1}^{+\bullet}$. Thus, the branching ratios for backbone dissociations should depend on the population of these excited states when formed by electron transfer and on the probability of such transitions, e.g., $(\mathbf{B})\mathbf{1a}^{+\bullet} \rightarrow (\mathbf{X})\mathbf{1e}^{+\bullet}$, and likewise for $(\mathbf{C})\mathbf{1a}^{+\bullet} \rightarrow (\mathbf{X})\mathbf{1i}^{+\bullet}$. Solving the kinetics for these isomerizations would require an extensive mapping of the PESs for the excited states of $\mathbf{1a}^{+\bullet}$ which is currently not feasible for systems of this size.

It is worth noting that both B3LYP and MP2 calculations agree that a direct dissociation of the Ala_1-Ala_2 N−C_α bond in the zwitterionic **X** state of $\mathbf{1a}^{+\bullet}$ (**TS3**) is not competitive with the proton migration through **TS1** or loss of ammonia through **TS9**. This finding is important because it addresses the chicken-and-egg question of the Utah−Washington mechanism of electron-induced peptide fragmentations referring to two alternative step sequences in the N−C_α bond dissociation.[49,50] One alternative postulates that the N−C_α bond cleavage occurs in the π^* zwitterionic state and is followed by a proton transfer.[47] This corresponds to the $\mathbf{1a}^{+\bullet} \rightarrow$ **TS3** pathway in Scheme S2. The other alternative postulates that the π^* zwitterion acts as a superbase and isomerizes by exothermic proton transfer to an aminoketyl intermediate.[48] This corresponds to the $\mathbf{1a}^{+\bullet} \rightarrow$ **TS1** $\rightarrow \mathbf{1d}^{+\bullet}$ pathway. The present analysis of the **X** state reaction kinetics in an experimentally studied peptide ion clearly prefers the superbase mechanism, in which a fast proton transfer is followed by a slower N−C_α bond cleavage. Nevertheless, it is still possible that the N−C_α bond cleavage may take place in one of the excited π^* states, where the initial N−C_α bond cleavage may be rate determining.

Contrasting the ECID and ETD dissociations, electron capture by the pentapeptide dications mainly triggers a hydrogen atom loss followed by charge-driven dissociations of singly protonated intermediates to give b_n fragment ions. The cation-radical dissociations can be explained by electron capture in electronic states corresponding to His imidazolium radicals which are expected to lose H atoms.[51] Loss of a H atom from the His radical ring can be particularly competitive at high internal energies acquired by ion−electron recombination (495−520 kJ mol^{-1}, Table 2), where dissociations with loose TSs are kinetically favored. For example, the TS for the loss of an imidazole hydrogen atom from $\mathbf{1b}^{+\bullet}$ (**TS10**, Figure S8, Supporting Information) is 73 kJ mol^{-1} above $\mathbf{1b}^{+\bullet}$. At an excitation corresponding to the recombination energy in $\mathbf{1a}^{2+} + e^- \rightarrow \mathbf{1b}^{+\bullet}$ (5.13 eV, 495 kJ mol^{-1}), the loss of H from the imidazole ring in $\mathbf{1b}^{+\bullet}$ is calculated to have a rate constant of 1.3×10^7 s^{-1} (Figure S8), which may be competitive with backbone cleavage dissociations.

At present, we can only speculate about the reason for the presumed formation of His-radical-like states upon ion−electron

(50) Chen, X.; Tureček, F. *J. Am. Chem. Soc.* **2006**, *128*, 12520–12530.
(51) Nguyen, V. Q.; Tureček, F. *J. Mass Spectrom.* **1996**, *31*, 1173–1184.

Scheme 3

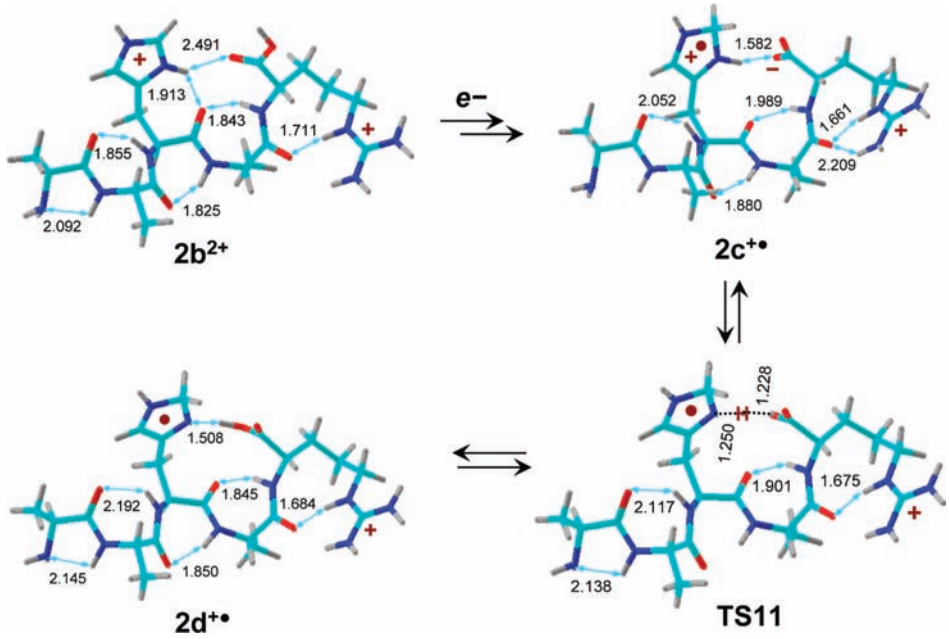

Scheme 4

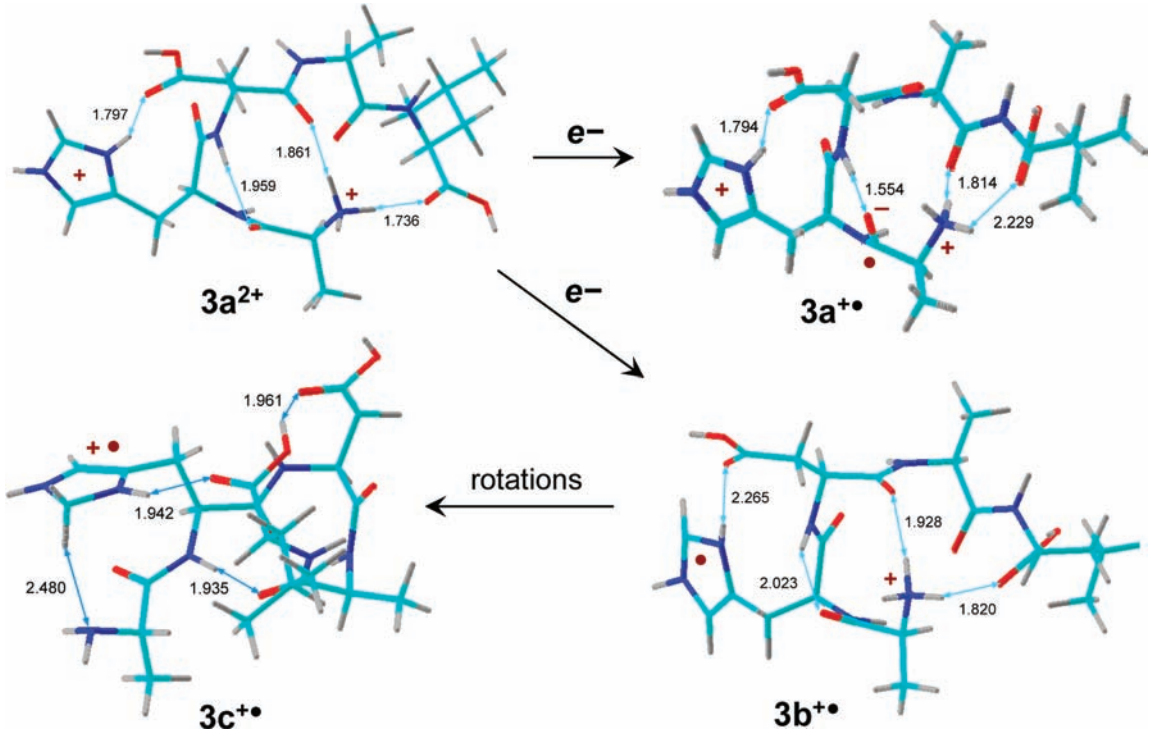

recombination. We note that the doubly protonated peptides have substantial dipole moments, e.g., 11.5 and 7.5 D for $\mathbf{1a}^{2+}$ and $\mathbf{2a}^{2+}$, respectively. The dipole moments in both $\mathbf{1a}^{2+}$ and $\mathbf{2a}^{2+}$ are aligned such that the positive pole is close to the His ring and the negative pole is close to the COOH group. This dipolar field creates a ~0.5 eV slant in the electrostatic potential along the His···COOH ion axis, as shown for $\mathbf{1a}^{2+}$ (Figure 6). This gradient steers the incoming free electron toward the His ring and favors its capture in an electronic state corresponding to a His ring radical. In contrast, electron transfer in ECID depends on the momentary orientation of the collision partners, which is sampled at random and is not affected by the dipolar field of the cation.

Cation-Radical Survivor Ions. The charge-reduced peptide cation-radicals from ECID/ETD showed a remarkable stability. Following collisional activation, the major radical-induced dissociation was loss of a $C_4H_6N_2$ neutral molecule (Figure 3). In accordance with previous studies of His-containing di- and tripeptides,[16,17] we propose a mechanism for the stabilization of the charge-reduced ions that involves proton migration to the His imidazolium ring, forming an imidazoline cation-radical. Depending on the peptide sequence and protonation pattern, the

source of the migrating proton can be the COOH or N-terminal ammonium groups. Among several migration mechanisms we studied, two are representative. Scheme 3 shows a spontaneous and exothermic COOH proton migration following charge reduction of $\mathbf{2b}^{2+}$. This forms a zwitterion ($\mathbf{2c}^{+\bullet}$) consisting of an imidazoline cation-radical and a carboxylate anion. Intermediate $\mathbf{2c}^{+\bullet}$ is in equilibrium with an imidazole radical ($\mathbf{2d}^{+\bullet}$), and these two tautomers are separated by a negligible energy barrier in **TS11** (Table 3). Radical $\mathbf{2d}^{+\bullet}$ is a reactant for the cleavage of the His $C_\alpha-C_\beta$ bond, leading to loss of $C_4H_6N_2$.

Scheme 4 shows stabilization in a cation-radical formed by electron transfer to the AHDAL ion $\mathbf{3a}^{2+}$. Two stable cation-radicals were identified as local energy minima. The more stable one ($\mathbf{3a}^{+\bullet}$) was a zwitterion in which the unpaired electron was contained within the Ala_1 amide group to give it pronounced anion-radical properties, while the positive charges were in the protonated N-terminal and His imidazole groups. The other cation-radical was a classical His radical ($\mathbf{3b}^{+\bullet}$). The finding that the zwitterion was more stable than the His radical (Table 3) again indicated that zwitterions represent low-energy structures for charge-reduced peptide cation-radicals. The His radical $\mathbf{3b}^{+\bullet}$ can undergo highly exothermic proton migration from the N-terminal ammonium to the imidazolium ring, forming an imidazoline cation-radical ($\mathbf{3c}^{+\bullet}$). The migration requires a conformational change by internal rotations but is barrierless in conformers allowing interaction between the N-terminal NH_3^+ group and the His imidazole radical. A similar exothermic isomerization involving the N-terminal ammonium can proceed in charge-reduced $\mathbf{1b}^{+\bullet}$ (see $\mathbf{1m}^{+\bullet}$, Scheme S6). The high exothermicity of these proton migrations is due to the very high basicity of the N-3-H imidazole radical for protonation at C-2′. For a model 4-methyl-N-3-H-imidazole radical, we calculate the proton affinity at C-2 as PA = 1047 kJ mol^{-1},[52] which substantially exceeds those of N-terminal amine group in small peptides[53] and imidazole (946 kJ mol^{-1}).[54]

Conclusions

This joint experimental and computational study revealed major differences between dissociations of pentapeptide cation-radicals induced by electron transfer from neutral and anionic targets on one hand and capture of a free electron on the other. Electron transfer gives rise to a number of electronic states in the charge-reduced peptides which differ in the electron density distribution and can explain the observed dissociations. In particular, several zwitterionic π^* amide states are found to be low-energy local minima which are comparably stable as the more usual histidine imidazolium radicals. The latter undergo facile isomerization of the imidazole ring which is catalyzed by proton transfer from the carboxyl or ammonium groups and results in substantial stabilization of the peptide cation-radicals. RRKM analysis of the loss of ammonia and backbone $N-C_\alpha$ bond dissociations induced by electron transfer indicates that these dissociations do not occur competitively and thus must originate from distinct reactants formed from different electronic states of charge-reduced peptide cation-radicals. In contrast, dissociations induced by capture of a free electron primarily involve loss of a hydrogen atom and presumably occur from reduced histidine radicals.

Acknowledgment. F.T. and T.W.C. thank Dr. Priska von Haller of the University of Washington Proteomics Resource Center for access to the Thermo LTQ-ETD and LTQ-FT-MS instruments. We also thank Dr. Iain Campuzano of Waters Corp. for ion mobility measurements. Research at University of Washington was supported by the NSF (Grants CHE-0750048 for experiments and CHE-0342956 for computations). The Department of Chemistry Computer Facility has been jointly supported by the NSF and University of Washington. F.T. also thanks the Department of Physics and Astronomy at Aarhus University, Denmark, for a Visiting Professor fellowship in July 2008, during which the above-described ECID experiments were carried out. Research at Aarhus University was supported by the Danish Natural Research Council (Grant 272-06-0427), Carlsbergfondet (Grant No. 2006-01-0229), and Lundbeckfonden. B.P. thanks the Deutsche Forschungsgemeinschaft for a Heisenberg Fellowship. B.B. thanks the DKFZ for a Guest Scientist Fellowship.

Supporting Information Available: Complete refs 24, 27b, and 29; Tables S1−S13, Figures S1−S9, and Schemes S1−S6. This material is available free of charge via the Internet at http://pubs.acs.org.

JA907808H

(52) From single-point CCSD(T)/aug-cc-pVTZ calculations on B3LYP/6-31+G(d,p) optimized geometries and using B3LYP/6-31+G(d,p) zero-point energies and enthalpies for 4-methyl-N-3-H-imidazole radical and its C-2-protonated form.

(53) Harrison, A. G. *Mass Spectrom. Rev.* **1977**, *16*, 201–217.
(54) NIST Standard Reference Database No. 69, March 6, 2009.